

# Large-Eddy Simulation of Turbulent Pulsating Jets

Eng. Mansour A K A S Aljaman

## ABSTRACT

*This paper presents the results of computer fluid dynamics simulation for synthetic and pulsating jets. ANSYS Fluent, a computer fluid dynamics package, is utilized to perform the planar, unsteady simulation. The large eddy simulation (LES) is selected as the turbulence model. The simulation results were analyzed in order to reveal some peculiarities of the flow.*

**KEYWORDS:** jets; ANSYS; unsteady ;large eddy; turbulence; flow

Date of Submission: 16-11-2021

Date of acceptance: 01-12-2021

## I. INTRODUCTION

Jets are noteworthy flows applied at performing many industrial tasks. Impinging jets are able to transfer high levels of heat. They have been studied in a diversity of configurations having various geometrical and dynamic parameters. Being indispensable on the study of Internal Combustion Engines (ICE) spray liquid and vapor penetration are subject to many experiments [1]. Much attention is also paid to research of injection process modeling [2]. The main objectives of this study are Large-Eddy Simulation (LES) [3] of turbulent pulsating planar jet [4] and synthetic jet [5] through ANSYS-FLUENT software and analysis of the LES simulation results.

## II. THE PHYSICS PROBLEM

Three-dimensional (3D) planar air jets are considered in this study. Two types of jets have been modeled:

- 1) Planar pulsating air jet with non-zero mean inflow velocity.
- 2) Planar pulsating air jet or 'synthetic jet' with zero mean inflow velocity.

In both cases the same computation domain is used which is represented at Figure 1. The computation domain size is  $L_x \times L_y \times L_z = 2m \times 4m \times 0.02m$ . The area of jet discharge is located in the middle of the lower side  $Y = 0$  of the computation domain. The size of the jet inlet area is equal to  $D = 0.1m$ . Mean velocity of the jet at the inlet boundary is  $10m/s$  and  $0m/s$ , respectively. At the rest of the lower boundary of the computation domain the walls were set with non-slip boundary condition. The symmetric boundary condition is set at the boundaries in z-direction. At the rest of the boundaries, pressure outlet boundary condition with zero pressure  $P_{outlet} = 0 [Pa]$  was set. The temperature in the computation domain is assumed to be uniform. All the simulations were carried out for incompressible liquid. At setting the jet inlet velocity  $V_{inlet}$  the following formulas were used:

1) In case of planar pulsating air jet with non-zero mean inflow velocity  $V_{inlet} = V[1+A \cdot \sin(2\pi f_0 t)]$ , where  $V = 10m/s$  is the mean inlet velocity,  $f_0 = 20 [Hz]$  is the pulsation frequency,  $t$  is time,  $A = 0.3$  is the pulsating amplitude.

2) Planar pulsating air jet 'synthetic jet' with zero mean inflow velocity  $V_{inlet} = V \cdot \sin(2\pi f_0 t)$ , where  $V = 10m/s$  is the mean inlet velocity,  $f_0 = 20 [Hz]$  is the pulsation frequency,  $t$  is time.

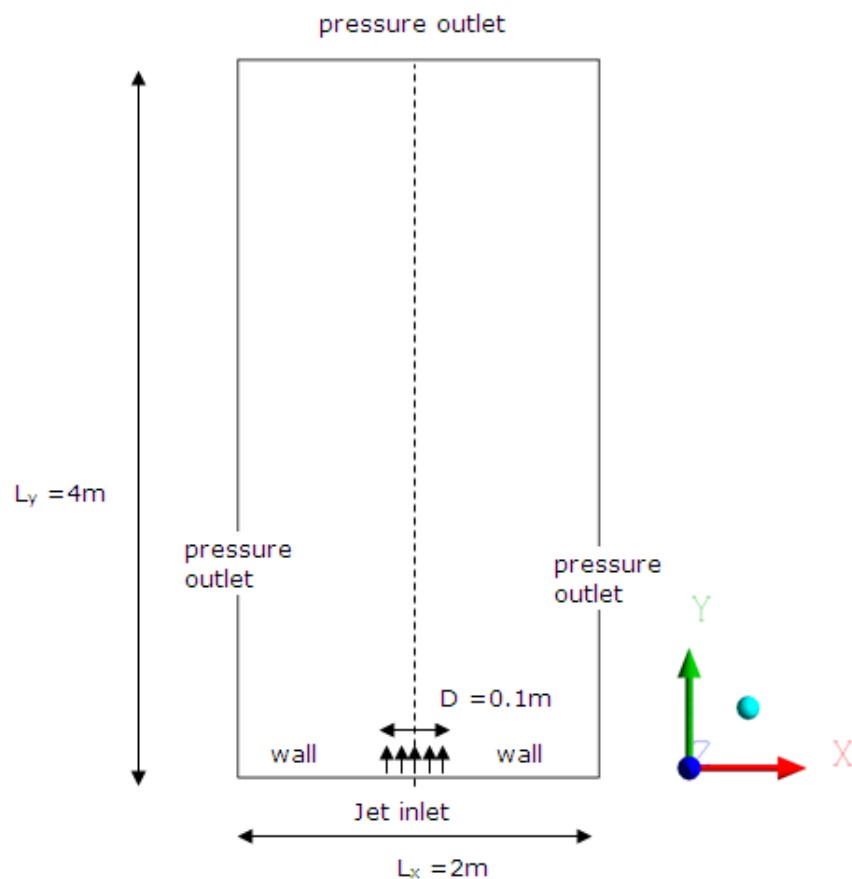


Figure 1. Computation Domain

### III. SIMULATION PARAMETERS

All the simulations within the report have been carried out with the use of the ANSYS Fluent 16.2 CFD code [6]. Within this code, the governing equations are written in a transient formulation and the incompressible fluid assumption is selected. The finite volume method for unstructured grids with a cell-centered data arrangement is adopted. The equations are solved through the implicit point Gauss-Seidel method using the Rhie-Chow flux correction [7] which is aimed at suppressing unphysical pressure oscillations. An algebraic multigrid solver is applied for convergence acceleration by computing corrections on a series of grids. The SIMPLEC method [8] is used for pressure velocity coupling, and 20 sub iterations per time step are performed. The inviscid fluxes in the momentum equations are approximated with the use of the second order centered scheme (CD). For pressure interpolation, the 'Standard' interpolation (weighted interpolation based on central coefficients) is utilized and the gradients are approximated with the use of cell-based Green-Gauss theorem. The time derivatives are approximated with the use of the three-level second order backward Euler scheme. The time step is equal to  $\Delta t = 4 \cdot 10^{-4}$  which leads to maximum local Courant number of about 0.9 for all computation domain. Simulation was run until  $t < t_{max} = 4s$ . As initial conditions zero fields of pressure and velocity were chosen.

Block-structured grid with hexahedral cells was constructed through ANSYS ICEM CFD [9], see Figure 2. The computational grid consists of 23793 hexahedral cells and has the following dimensions:  $N_x \times N_y \times N_z = 80 \times 310 \times 2$ . Out of 80 X grid points, 28 grid points are attributed to the inlet of the jet. The grid points are distributed the way to ensure the maximum aspect ratio (ratio of two cell sides in XY plain) in the jet area be less or equal to 2. The cells are prolonged along the line of Y. Notably, LES requires using three-dimensional computational grids, that's why in the third direction 2 computation points were set to ensure three-dimensionality of the computation grid.

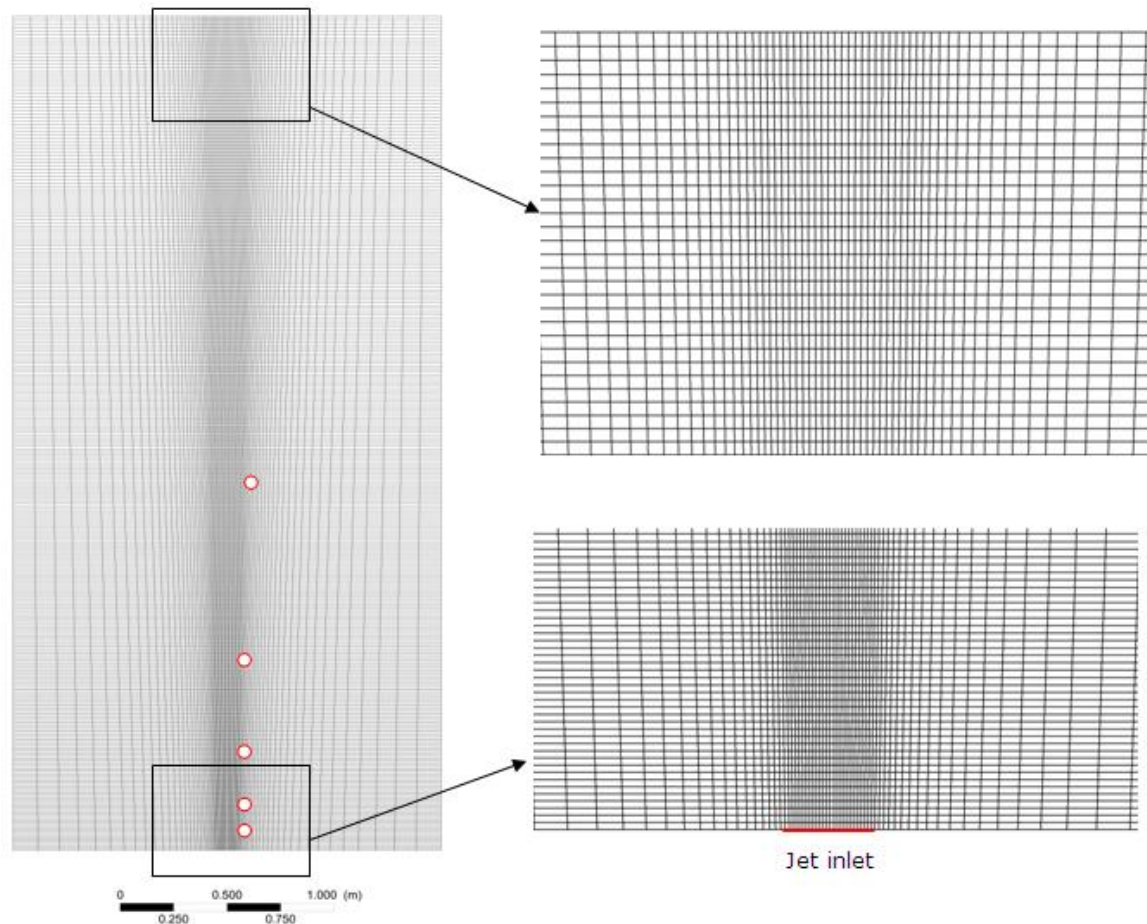


Figure 2. Grid and its Fragments

To set the inlet velocity the following user define functions (UDF) were applied [10]:

- 1) In case of planar pulsating air jet with non-zero mean inflow velocity  
#include "udf.h"

```

DEFINE_PROFILE(inlet_velocity, thread, position)
{
    float t, A, velocity, V, Pi, f0;
    face_t f;
    t = RP_Get_Real("flow-time");
    V = 10.0;
    A = 0.3;
    Pi = 3.1415926535897932384626433832795;
    f0 = 20;
    velocity = V*(1+A*sin(2*Pi*f0*t));

    begin_f_loop(f, thread)
    {
        F_PROFILE(f, thread, position) = velocity;
    }
    end_f_loop(f, thread)
}

```

- 2) In case of "synthetic jet" with zero mean inflow velocity, line " $velocity = V*(1+A*\sin(2*Pi*f0*t));$ " was replaced by " $velocity = V*\sin(2*Pi*f0*t);$ ".

IV. RESULTS DISCUSSION

For detailed description of nonstationary structure of planar pulsating air jet for each case the fields of axial velocity component and velocity curl Z component were constructed, as well as velocity magnitude dependency diagrams and their energy spectra (obtained through Fourier decomposition) for 5 monitoring points. All the monitoring points are located at the conventional boundary of the jet with Y-coordinate equal to 0.5D from the center of the jet (geometrical center of the computational domain). For the monitoring points the following values of X-coordinate were chosen: 1D, 2D, 4D, 8D, 16D. Conventional position of the monitoring points is represented at figure 2 as blank circles (○).

4.1. Case 1: Planar Pulsating Air Jet with Non-Zero Mean Inflow Velocity

Figure 3 shows the fields of velocity magnitude for three time points. Figure 4 represents the fields of velocity curl Z component for three time points. Figure 5 represents dependency of axial velocity component on time for five monitoring points. Figure 6 shows energy spectra of graphs 5, obtained through Fourier decomposition.

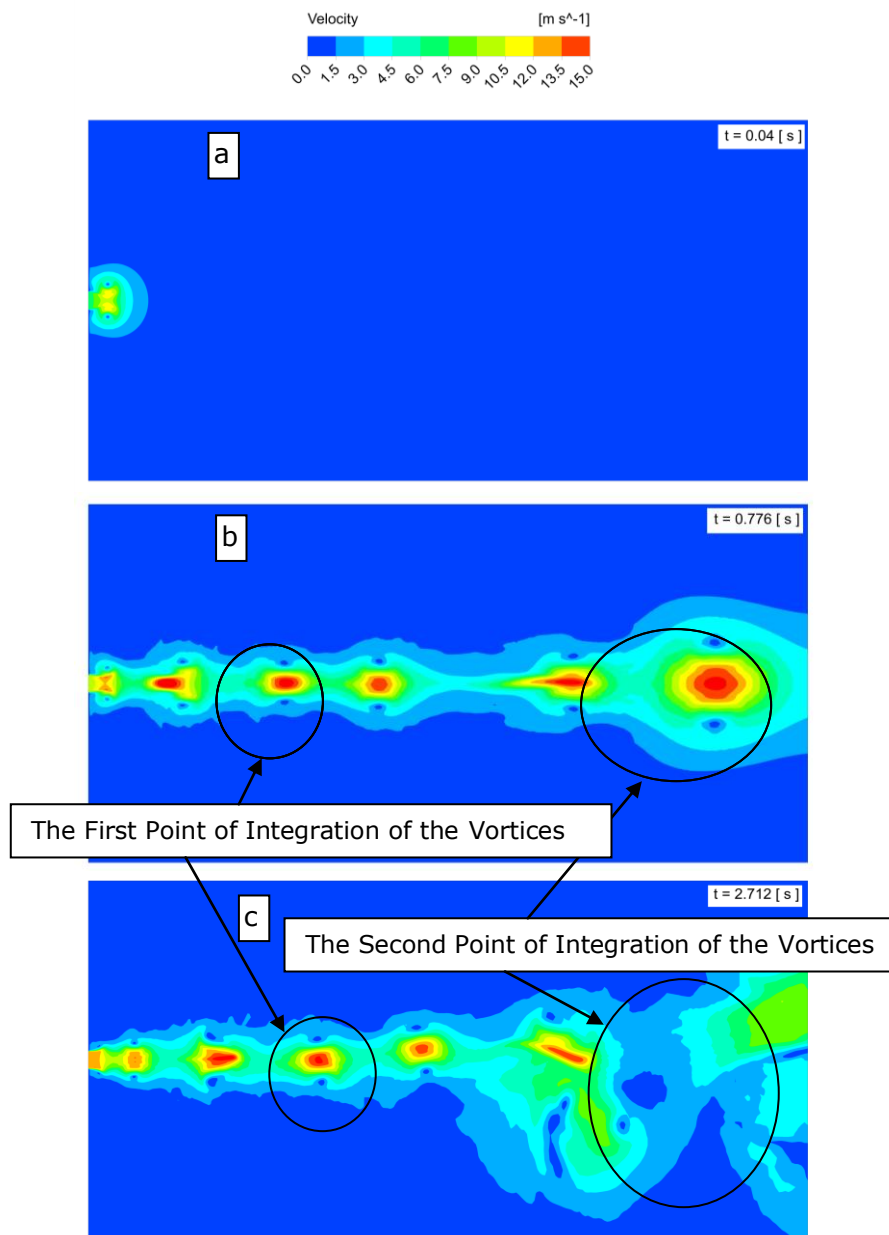


Figure 3. Fields of Velocity Magnitude for Three Time Points

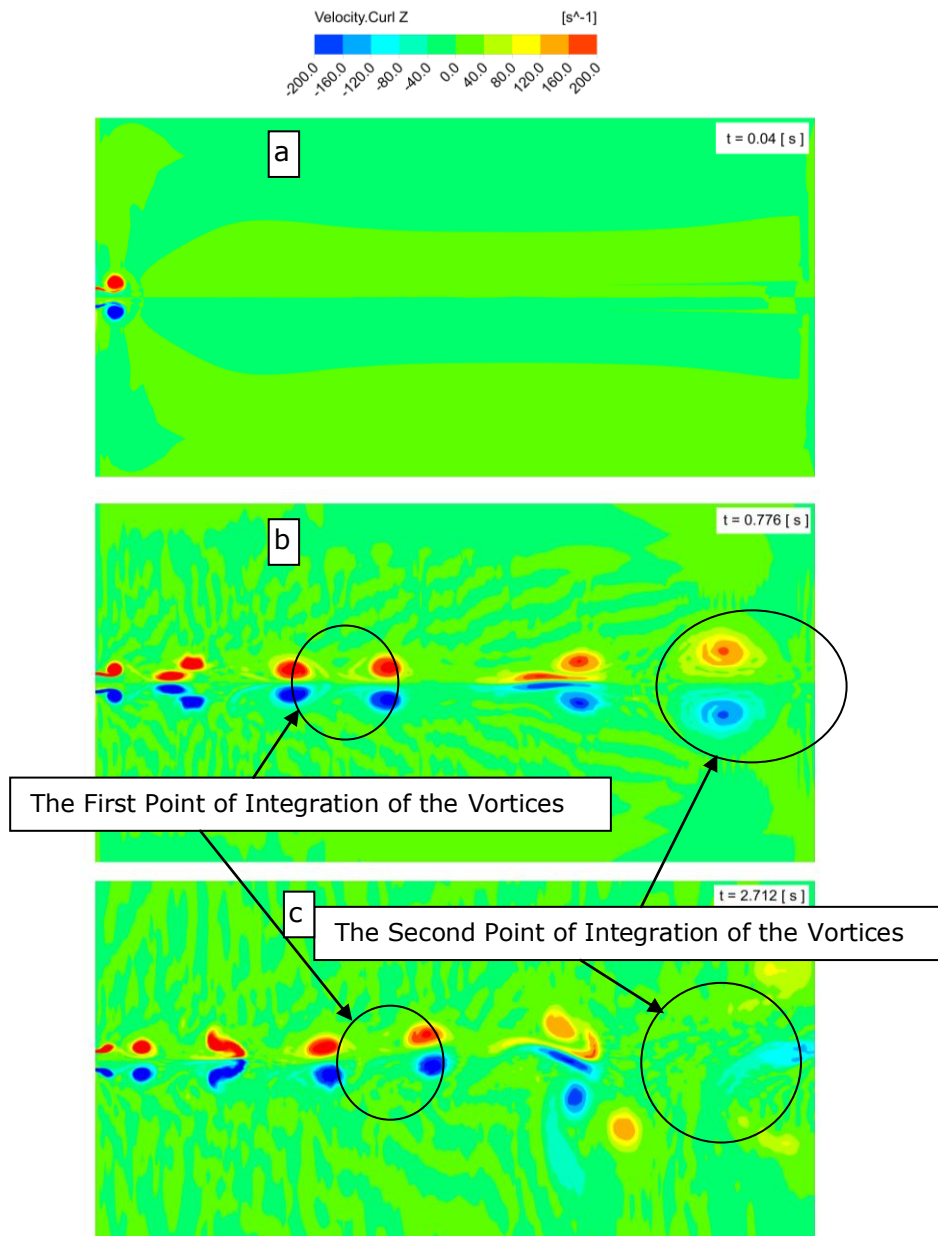
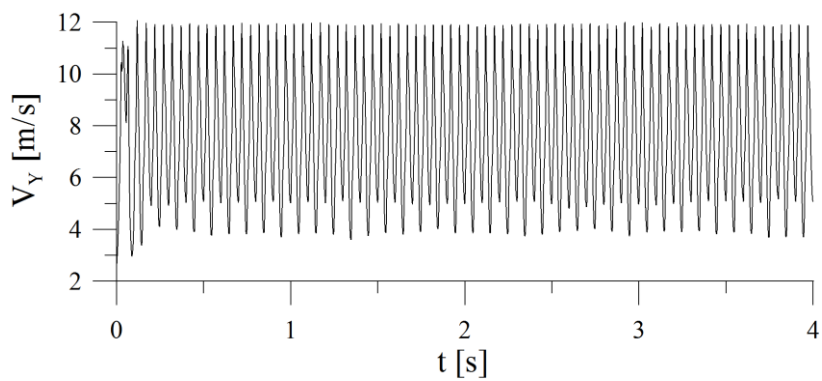


Figure 4. Vorticity Fields (Velocity Curl Z Component) for 3 Time Points



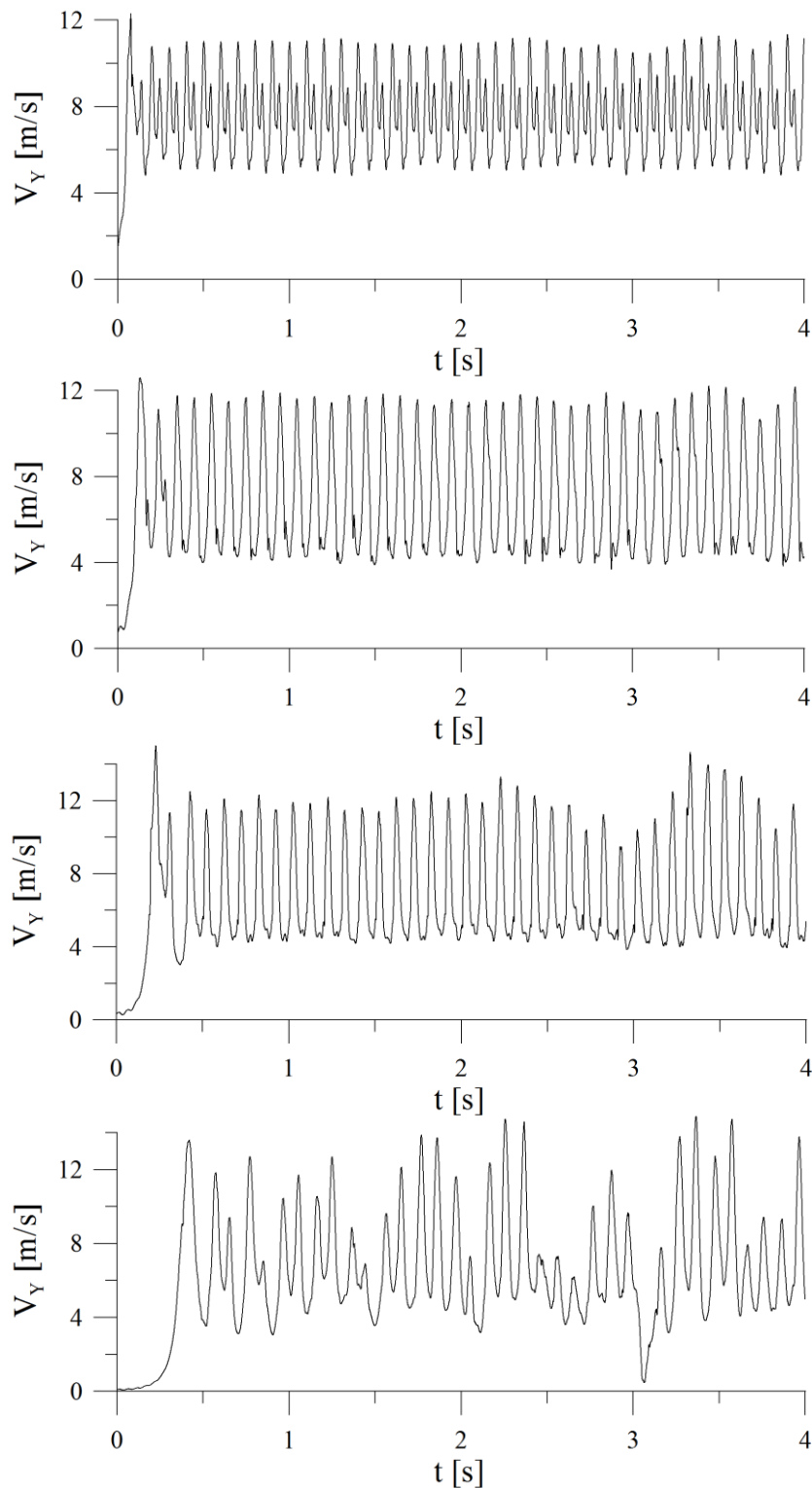


Figure 5. Dependency of Axial Velocity on Time for Five Monitoring Points

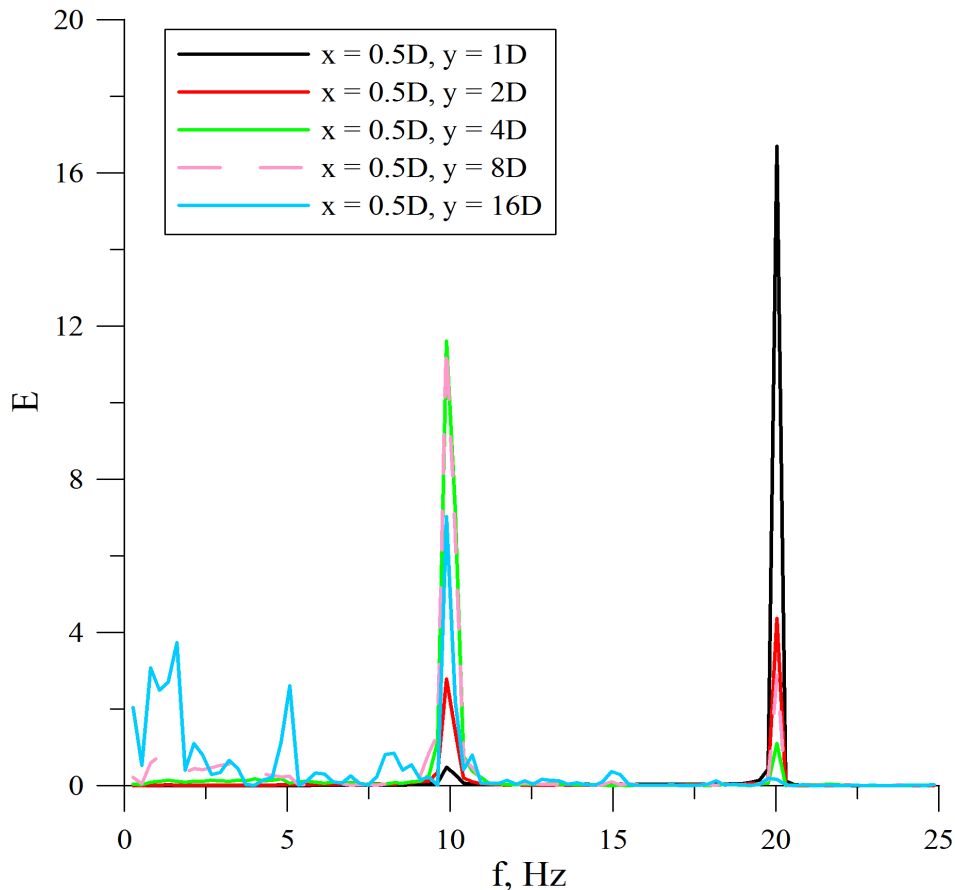


Figure 6. Energy Spectra of Axial Velocity

One may conventionally separate two time periods:

- Initial period  $t = 0.0 - 0.9s$ . This is the period of flow formation, when initial stable vortex structures are being formed. These vortex structures are shown at figures 3b and 4b. One may see there pairs of vortices flowing from the inlet section of the jet with the frequency equal to the frequency of the perturbances applied to the jet  $f_0 = 20Hz$ . Figures 4a and 5a present initial time point, when formation of the first pair of vortices occurs and they flow into the undisturbed space where all the values are equal to zero. At figures 3b and 4b one may observe pairwise integration of the vortex structures. This process takes place twice: first, the vortex structures formed at the inlet of the jet are integrating into larger structures, and then these larger vortex structures are integrating for the second time, as represented at figures 3b, 4b.
- Developed flow  $t = 0.9 - 4s$ . In this time period vortex structures have already been fully developed and the flow is of periodic nature. At the section  $X = 0.0D - 9.0D$  the vortex structures maintain stability. Further down the flow the jet loses its stability. One may observe oscillating deviation of the jet from the axis. One may also observe pairwise integration of the vortex structures. This process takes place twice: first, the vortex structures formed at the inlet of the jet are integrating into larger structures, and then these larger vortex structures are integrating for the second time, see figures 3c, 4c.

These observations are proved with the analysis of images of the energy spectra (figure 6) of the flow and the diagrams of dependency of axial velocity component on time (figure 5). Where in monitoring point 1, approximated to the inlet boundary one may see only the basic frequency equal to  $f_0 = 20Hz$ , in monitoring points 2, 3, 4 one may observe basic frequency  $f_0 = 20Hz$  and additional frequency  $f_1 = 10Hz$ , and in monitoring point 5 there is frequency  $f_1 = 10Hz$  and  $f_2 = 5Hz$ . Presence of frequency  $f_1$  evidences the integration of two 'basic' vortex structures into a larger one. Presence of frequency  $f_2$  evidences further integration of the pairs of larger vortex structures.

#### 4.2. Case 2: Planar Pulsating Air Jet with Zero Mean Inflow Velocity

Figure 7 represents the fields of velocity magnitude for three time points. Figure 8 shows the field of velocity curl Z component for three time points. Figure 9 shows the diagrams of dependency of axial velocity component

on time for 5 monitoring points. Figure 10 shows energy spectra of diagrams 9, obtained through Fourier decomposition.

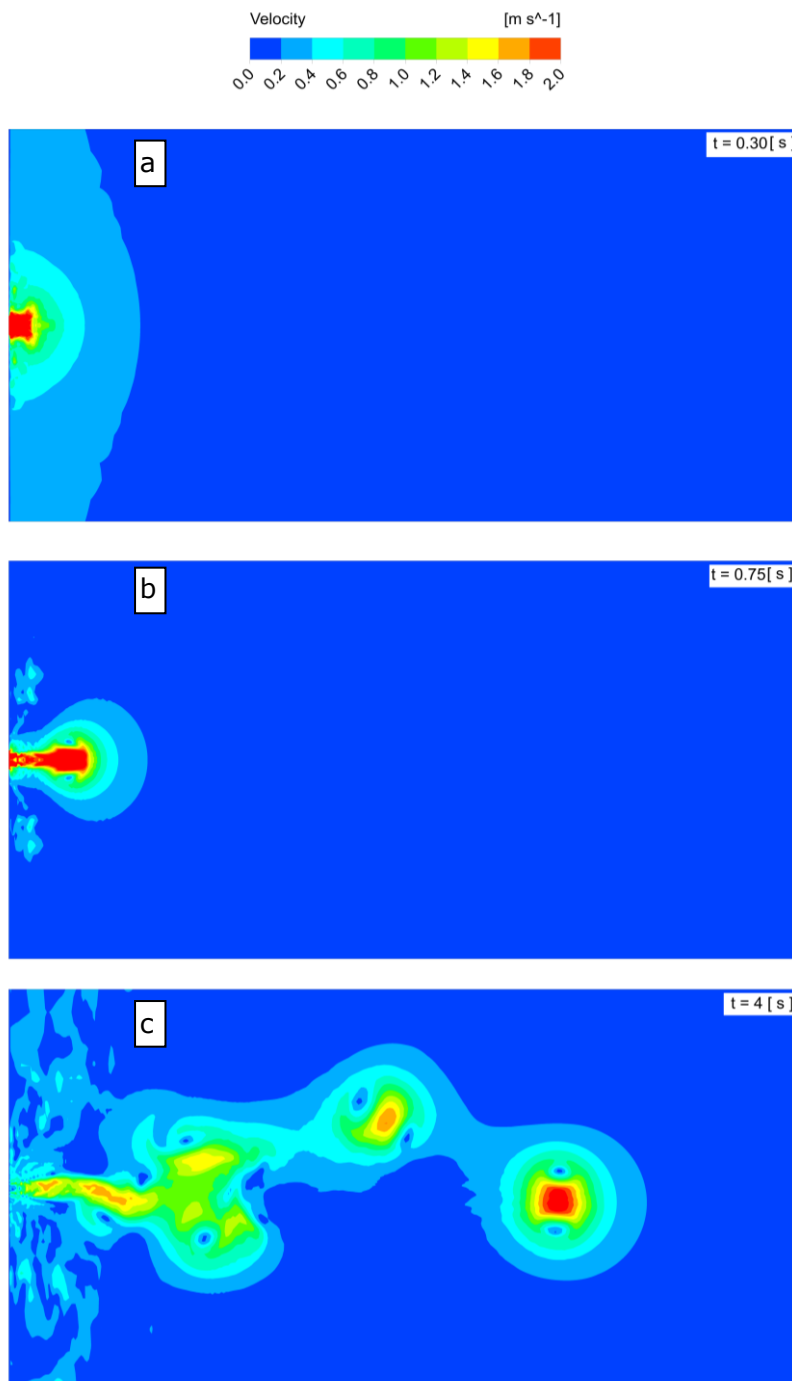


Figure 7. Fields of Velocity Magnitude for Three Time Points

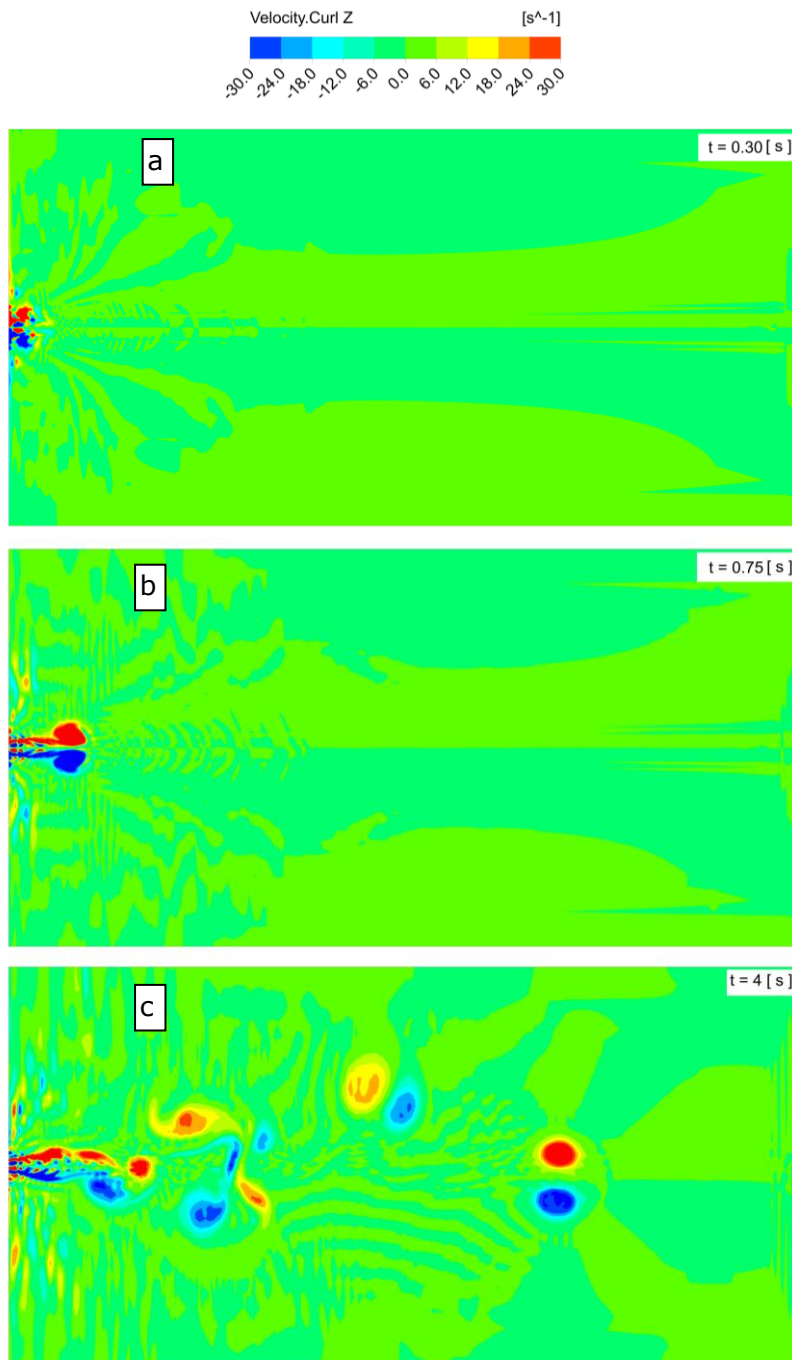


Figure 8. Fields of Velocity Curl Z Component for 3 Time Points

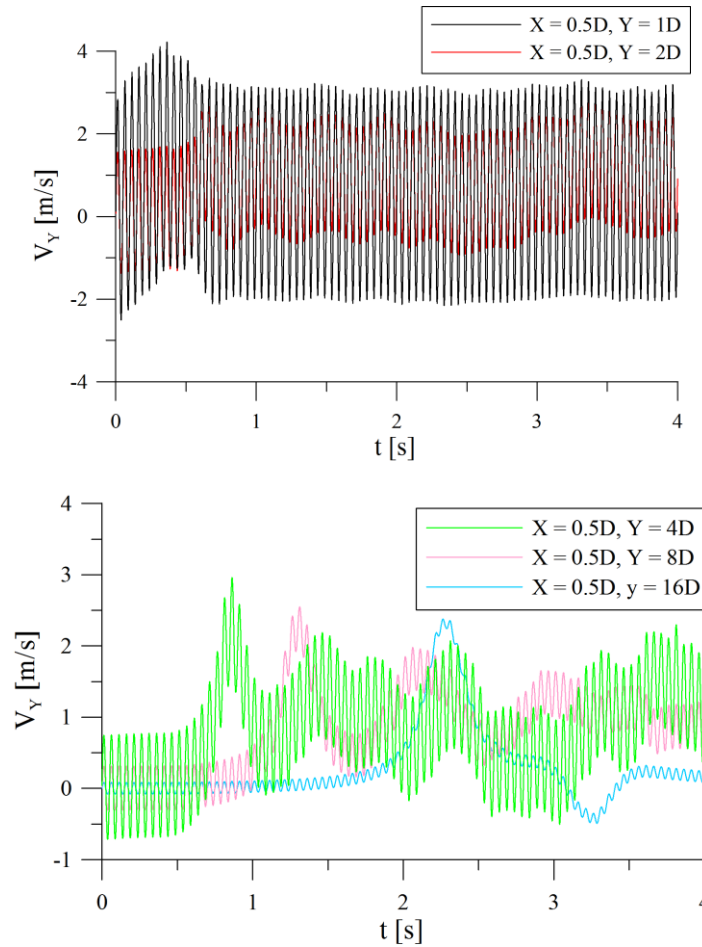


Figure 9. Dependency of Axial Velocity on Time for Five Monitoring Points

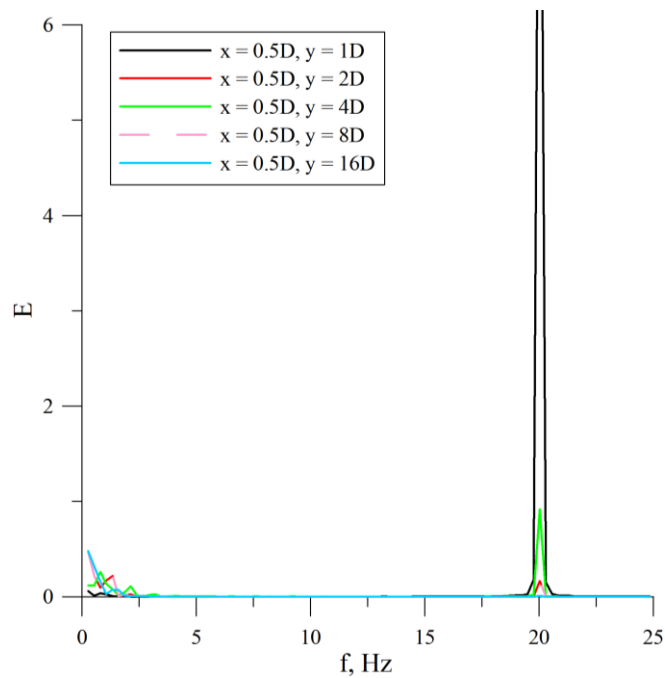


Figure 10. Energy Spectra of Axial Velocity

Synthetic jet does not make high impact on external environment. Figures 7a and 8a represent the fields of velocity magnitude and velocity curl Z component at time point  $t = 0.3s$ . At time point  $t = 0.75s$  the pair of weak vortices starts spreading from the inlet boundary into the computational domain as represented at figures

7b and 8b. Further, periodic efflux of impulses as a pair of vortices takes place which is shown at figure 7c and 8c. The vortices spread along the computation domain chaotically. These observations are proved by the analysis of images of energy spectra (figure 10) of the flow and the diagrams of dependency of axial velocity component on time (figure 9). The diagrams of energy spectra show presence of only one frequency  $f_0 = 20Hz$ . One may also observe decay of oscillations at distancing from the jet inlet.

## V. CONCLUSION

Large-Eddy Simulation of turbulent pulsating planar jet and synthetic jet were performed using ANSYS-FLUENT software and the LES simulation results were analyzed.

The following peculiarities of pulsating jet flow were revealed:

- 1) Periodic formation of a pair of vortices twirling to opposite ways at the inlet of the pulsating jet. The frequency of the vortices pair formation coincides with the frequency of the jet pulsation  $f_0 = 20Hz$ ;
- 2) Pairwise integration of vortices. One may observe two integrations of the vortices. At first a pair of vortices released by the jet integrates with the pair of the same vortices released by the jet a little bit earlier in time, which results in formation of a pair of larger vortices. Then the same pairwise integration of larger vortices takes place. This process explains emergence of additional frequencies in the Fourier spectrum  $f_1 = 10Hz$  and  $f_2 = 5Hz$ ;
- 3) The section of stable flow is revealed, where the axis of the jet does not deviate from the geometric axis of the computational domain,  $L = 0.0D-9.0D$ ;
- 4) The time point of the jet stability is defined, where the axis of the jet starts deviating from the geometric axis of the computational domain,  $T = 0.0s - 0.9s$ .

The following peculiarities of the flow for synthetic jet were revealed:

- 1) Weak impact of synthetic jet on the external environment;
- 2) Formation of a pair of weak vortices at the jet inlet;
- 3) Lack of the processes of the vortices pairwise integration.

## REFERENCES

- [1]. Abraham, J., "What is Adequate Resolution in the Numerical Computations of Transient Jets," SAE Technical Paper 970051, 1997, doi:10.4271/970051.
- [2]. Sirignano William A., Fluid Dynamics of Spray – 1992 Freeman Scholar Lecture. Journal of Fluids Engineering, 1993 Vol.115/345.
- [3]. Kim, S.E., 2004. Large Eddy Simulation Using an Unstructured Mesh Based Finite-Volume Solver. AIAA Paper, 2004-2548.
- [4]. Jambunathan K., Lai E., Moss M. A. and Button B. L. [1992], A review of heat transfer data for single circular jet impingement, Int. J. Heat and Fluid Flow, Vol. 13, No. 2106-115
- [5]. Jet Theory B. Smith, A. Glezer, The Formation and Evolution of Synthetic Jets, Phys. Fluids 10 (9) (1998) 2281–2297.
- [6]. Ansys Fluent Theory Guide, ANSYS, Inc, Release 15.0, November 2013, 780 p.
- [7]. Rhie, C.M. & Chow, W.L., 1983. Numerical Study of the Turbulent Flow Past an Airfoil with Trailing Edge Separation. AIAA Journal, 21(11), pp.1525–1532.
- [8]. Patankar, S.V., 1980. Numerical Heat Transfer and Fluid Flow
- [9]. Icem User's Manual, ANSYS, Inc, Release 15.0, November 2013, 78 p.
- [10]. Ansys Fluent UDF Manual ANSYS, Inc, Release 15.0, November 2013, 564 p.